the plant journal

SEB SOCIETY FOR EXPERIMENTAL BIOLOGY

The Plant Journal (2020) doi: 10.1111/tpj.14877

TECHNICAL ADVANCE

Affordable and robust phenotyping framework to analyse root system architecture of soil-grown plants

Thibaut Bontpart[1,†], Cristobal Concha[1,†], Mario Valerio Giuffrida[2,3,†], Ingrid Robertson[1,†], Kassahun Admkie[4], Tulu Degefu[5], Nigusie Girma[4], Kassahun Tesfaye[6,7], Teklehaimanot Haileselassie[6], Asnake Fikre[4,5], Masresha Fetene[6,8], Sotirios A. Tsaftaris[2,*] and Peter Doerner[1,*]

[1]*Institute of Molecular Plant Science, School of Biological Sciences, University of Edinburgh, Max Born Crescent, Edinburgh, Midlothian, EH9 3BF, UK,*

[2]*Institute for Digital Communications, School of Engineering, University of Edinburgh, Edinburgh, Midlothian, EH9 3FG, UK,*

[3]*School of Computing, Edinburgh Napier University, Merchiston Campus, Edinburgh EH10 5DT, UK,*

[4]*Ethiopian Institute of Agricultural Research, Debre Zeit, Oromia, PO Box 32, Ethiopia,*

[5]*ICRISAT-Ethiopia, International Crops Research Institute for the Semi-Arid Tropics, c/o ILRI Campus, Addis Ababa, Addis Ababa, PO Box 5689, Ethiopia,*

[6]*College of Natural Sciences, Addis Ababa University, Addis Ababa, Addis Ababa, PO Box 1176, Ethiopia,*

[7]*Ethiopian Biotechnology Institute, Addis Ababa, Addis Ababa, PO Box 5954, Ethiopia, and*

[8]*Ethiopian Academy of Sciences, Addis Ababa, Addis Ababa, PO Box 32228, Ethiopia*

Received 17 December 2018; accepted 15 May 2020.

*For correspondence (e-mails peter.doerner@ed.ac.uk; S.Tsaftaris@ed.ac.uk).

[†]These authors contributed equally to this work.

SUMMARY

The phenotypic analysis of root system growth is important to inform efforts to enhance plant resource acquisition from soils; however, root phenotyping remains challenging because of the opacity of soil, requiring systems that facilitate root system visibility and image acquisition. Previously reported systems require costly or bespoke materials not available in most countries, where breeders need tools to select varieties best adapted to local soils and field conditions. Here, we report an affordable soil-based growth (rhizobox) and imaging system to phenotype root development in glasshouses or shelters. All components of the system are made from locally available commodity components, facilitating the adoption of this affordable technology in low-income countries. The rhizobox is large enough (approximately 6000 cm^2 of visible soil) to avoid restricting vertical root system growth for most if not all of the life cycle, yet light enough (approximately 21 kg when filled with soil) for routine handling. Support structures and an imaging station, with five cameras covering the whole soil surface, complement the rhizoboxes. Images are acquired via the Phenotiki sensor interface, collected, stitched and analysed. Root system architecture (RSA) parameters are quantified without intervention. The RSAs of a dicot species (*Cicer arietinum*, chickpea) and a monocot species (*Hordeum vulgare*, barley), exhibiting contrasting root systems, were analysed. Insights into root system dynamics during vegetative and reproductive stages of the chickpea life cycle were obtained. This affordable system is relevant for efforts in Ethiopia and other low- and middle-income countries to enhance crop yields and climate resilience sustainably.

Keywords: image-based plant phenotyping, root system architecture, rhizobox, *Cicer arietinum*, Raspberry Pi, Phenotiki, technical advance.

INTRODUCTION

The spatial distribution of plant roots is referred to as root system architecture (RSA), which changes over time as the plant grows and adapts to soil conditions (de Dorlodot *et al.*, 2007; Tian and Doerner, 2013). Many different approaches are used to characterize RSA. Analysis can focus on parameters such as the shape and expanse of the root system: i.e. its *spatial distribution* in the soil.

Alternatively, the use of *topological* parameters results in a generalized representation of root hierarchies: the main root develops first (the primary root, PR), from which branches emerge (the secondary roots, SRs), with further branches emerging from the SRs (the tertiary roots, TRs), and so on (Lynch, 1995). Most dicotyledonous plants develop a root system in which roots can be readily parsed in this manner, whereas monocotyledonous plants exhibit a more complex system that defies simple hierarchical characterization as they generally lack a clear main root (Smith and De Smet, 2012; Atkinson *et al.*, 2014). The above approaches can also be complemented by analysis of individual root *morphology*, for example, root diameter (Lynch, 1995).

Roots not only provide anchorage but also acquire resources (water and nutrients), and for both of these functions the spatial distribution of the root system within the soil is a critical determinant of the successful exploitation of below-ground resources, most of which are non-uniformly distributed (Giehl and von Wiren, 2014). Therefore, topology and morphology are necessary but insufficient descriptors of root systems (Lynch, 1995). Root system growth in the soil gives rise to emergent system parameters: for example, the convex hull, defined as the area of the smallest polygon, with interior angles $\leq 180°$, covering the whole root system, when projected onto a 2D plane (Pound *et al.*, 2013). As the spatial distribution of the root system in the soil, the RSA both describes the plant resource acquisition capacity, and ensuing competitive success (Padilla *et al.*, 2013), and provides physical evidence of the resource investment strategies that the individual plant has adopted.

RSA descriptors can be used for comparative purposes (Kutschera and Lichtenegger, 1997; Bouma *et al.*, 2001; Pages, 2016) and, because they relate to root system function, can inform crop improvement (Burridge *et al.*, 2016; Burridge *et al.*, 2017; Morris *et al.*, 2017). Emergent RSA parameters relate to the RSA at any moment in time, and extending this analysis to a time series also reveals important features, such as global or local growth patterns, and branching rates, that inform on the plant's resource capture and internal resource distribution strategies. For RSA analysis to contribute to plant improvement efforts, it must be simple, provide high throughput and be placed into the hands of those that require this information to develop better-performing lines (Lynch, 1995, 2007; Burridge *et al.*, 2016).

Soil opacity is a major problem when studying plant RSA. Modern techniques, such as X-ray computed tomography (Heeraman *et al.*, 1997; Morris *et al.*, 2017), allow for the three-dimensional (3D) reconstitution of the root system, even when grown in soil, but are slow, have limits on the soil volume that can be sampled and require prohibitively expensive equipment. For this reason, many lab-based growth systems have been developed that are geared towards visualizing root systems and their RSA with visible wavelength imaging, including growth matrices such as gellan gum (Iyer-Pascuzzi *et al.*, 2010), transparent synthetic soil (Downie *et al.*, 2012) and hydroponics (Mathieu *et al.*, 2015). In these cases, roots are not developing, growing or interacting with the natural abiotic and biotic environment in which they evolved (Morris *et al.*, 2018), and there is evidence that root growth behaviour in these systems differs from that of soil-grown plants (Rellan-Alvarez *et al.*, 2015; Silva-Navas *et al.*, 2015). Hence, when developing a plant growth system to study RSA parameters, one faces a trade-off between realistic growth conditions and root visibility.

Several investigators have attempted to combine the ease of root system detection and growth in a soil substrate. The first investigator known to have developed a 'root box' was Julius von Sachs in the 19th century (Sachs, 1865; Kutschera, 2015). Since then, many soil-based growth systems, referred to as *rhizoboxes*, have been developed, several of which allow observation of only a small fraction of the root system growing in 3D by introducing transparent tubes into the soil (Sanders and Brown, 1978). Other soil-based growth systems provide relatively thin layers of soil bordered by one or two transparent surfaces to visualize roots pressed against them, thus collapsing a variable fraction of the entire root system in 3D against a transparent surface for 2D representation (Neumann *et al.*, 2009). Such 2D systems have been reported for the dicotyledonous species *Arabidopsis thaliana* (Devienne-Barret *et al.*, 2006; Rellan-Alvarez *et al.*, 2015), *Solanum lycopersicum* (tomato; Dresbøll *et al.*, 2013; Rellan-Alvarez *et al.*, 2015), *Lupinus albus* (Lupine; Leitner *et al.*, 2014), and *Beta vulgaris* (sugar beet; Bodner *et al.*, 2017), or for monocots such as *Oryza sativa* (rice; Price *et al.*, 2002; Shrestha *et al.*, 2014), and *Triticum aestivum* (wheat; Jin *et al.*, 2015). These systems have allowed for the testing of plant growth behaviour in waterlogging (Dresbøll *et al.*, 2013) or low moisture stress (Avramova *et al.*, 2016; Durand *et al.*, 2016), or with contrasting nutrient availability conditions (Jin *et al.*, 2015). With the exception of two previous studies (Shrestha *et al.*, 2014; Jin *et al.*, 2015), the growth systems for such studies were ≤ 1 m in height (Rellan-Alvarez *et al.*, 2015; Avramova *et al.*, 2016), which limited analyses to the early growth phases of most plants. Although the constrained growth in such containers is distinct from plant growth in the field, the results obtained are informative and robotic systems for root phenotyping have been developed in for such platforms (Nagel *et al.*, 2012; Wu *et al.*, 2018). A frequent drawback of these systems is their substantial cost, arising from the use of bespoke or expensive components, that preclude their use at larger scales or implementation in low-income countries.

Two-dimensional (2D) growth systems enable the acquisition of root system images using flat-bed scanners (Devienne-Barret *et al.*, 2006), charge-coupled device (CCD)

camera(s) (Rellan-Alvarez *et al.*, 2015) or neutron radiography (Leitner *et al.*, 2014). To quantify and analyse RSA parameters, numerous software packages such as SMART-ROOT (Lobet *et al.*, 2011), GLO-RIA (Rellan-Alvarez *et al.*, 2015), ROOT SYSTEM ANALYZER (Leitner *et al.*, 2014), BRAT (Slovak *et al.*, 2014), ROOTTRACE (Naeem *et al.*, 2011) and EZ-ROOT-VIS (Shahzad *et al.*, 2018) have been developed. Many of these approaches are based on destructive analysis, however, or require artificial substrates and significant human intervention by highly trained operators (Kuijken *et al.*, 2015).

In this study, our objective was to develop a simple and affordable system composed of commodity components that are readily sourced in most parts of the world. We developed a large rhizobox (150 × 45 × 0.6 cm) developed to grow plants in soil and analyse their changing patterns of RSA. Our rhizobox was optimized to observe a large fraction of the root system in 2D. Critically, we accompany our rhizobox design with a purposefully designed and built imaging station, also based on affordable commodity components, to permit the acquisition of high-resolution images (approximately 9000 × 2700 pixels) using low-cost cameras. A set of RSA parameters were quantified until 7 weeks for *Cicer arietinum* (chickpea), providing unprecedented information about root system growth and development during the reproductive phase. To evaluate the robustness and utility of the system in different environments, the rhizobox system developed in Edinburgh, UK, was also established and tested at the Debre Zeit Agricultural Research Centre, Bishoftu, Ethiopia, using two chickpea cultivars commonly grown in Ethiopia.

RESULTS

Establishing a commodity component-based system to visualize soil-grown plant root systems

A modular, commodity component-based rhizobox was designed, assembled (Figure 1a,b; for blueprints, see http://chickpearoots.org/resourcesandlinks) and evaluated for chickpea and *Hordeum vulgare* (barley) growth in soil (Figure 1c). Each rhizobox, held in a supporting rack (Figure 1c), contained one plant and approximately 3700 cm^3 of soil in a 6-mm-thick layer. Rhizoboxes were imaged every 2–3 days until the bud emergence or pod-filling stages for chickpea with an imaging station that contained five Raspberry Pi cameras (Figure S1). Raw image data were processed in a procedural pipeline to assemble composite images for each root system at a given time point (Figure S2). From these images, the following emergent root system parameters were analysed: total area, convex hull area, total length, growth rate, depth, width, centroid, solidity and density (Table 1). Detailed information for rhizobox components and assembly, plant growth conditions and data capture are presented in the Experimental procedures and in Data S1.

Maximizing the measured fraction of the root system

Combined influence of soil compression and rhizobox inclination on root system visibility. To optimize the visible fraction of the root system on the anterior glass side and minimize data loss caused by roots not growing against this side, we built modified rhizoboxes by replacing the posterior polyvinyl chloride (PVC) sheet with a second glass pane (termed double-glass rhizoboxes), for which we could capture images from both sides in order to assess reliably the fraction of the root system exposed to the not normally visible back side.

We tested two soil compression methods: against the side facing downwards (anterior compression, against the front glass side) or against the side facing upwards (posterior compression, against the back side, which is normally PVC but in this experiment is glass), as well as two inclination angles of 30° and 45° from the vertical (Figure S3a). At 48 days after sowing (DAS) we acquired images of both sides and analysed the root system. The overlap of segmented images from the anterior and posterior sides (Figure S3b,c) illustrates the visibility of the root system in the worst (anterior 30°) and best (posterior 45°) conditions, respectively. The percentage of root pixels counted on each side (front in blue, back in orange) compared with the total number of pixels counted per rhizobox ($n = 4$ for each condition; Figure S3d) and mean percentage of the four rhizoboxes per condition (Figure S3e) reflect this. With compression against the anterior side and an inclination of 30°, only 42% of the roots were observed on the front side. At an inclination of 45°, 53.5% of the root system was visible on the front side. When the soil was compressed against the posterior side, the fraction of the root system visible on the front side reached a mean of 73.3 and 75.4% at inclinations of 30° and 45°, respectively. The lowest front side root system visibility of the rhizobox at an inclination of 45° was 69.7%, whereas it was 59.3% for the rhizobox at an inclination of 30° (Figure S3f). The posterior 45° condition resulted in higher maximal front visibility (86.2%), compared with a maximum of 79.2% for the posterior 30° condition (Figure S3d).

Although these differences (between posterior compression at 30° and 45°, respectively) in the observable (front) fraction of the root system were not statistically significant (Student's *t*-test, $P = 0.74$), we concluded that compression against the posterior side and an inclination of 45° were the best conditions to maximize the visible fraction of the root system in the rhizobox.

Data loss and data accuracy. In a separate experiment, we determined how much data we were missing by only assessing the anteriorly visible fraction in the default single-glass rhizoboxes. We used double-glass rhizoboxes to measure the visible root system on anterior and posterior

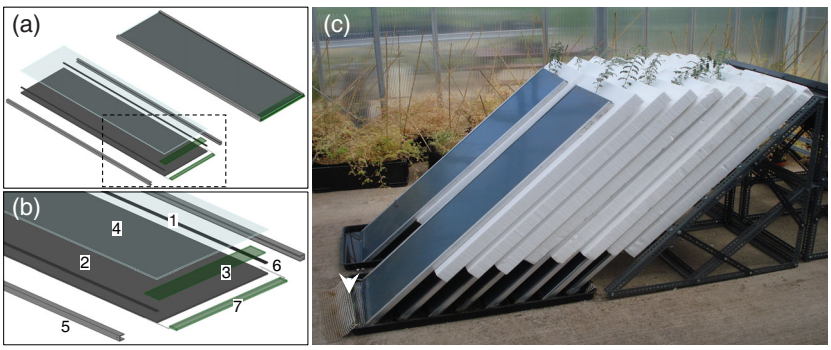

Figure 1. Rhizobox components and support. Exploded (a, left) and closed (a, right) view diagram of a rhizobox designed with FreeCAD 0.16. The enlarged exploded view (b) shows silicon strips (1) glued along the PVC sheet (2) laid horizontally. An inner piece of nylon mesh (3) is inserted at the base before soil loading. The glass pane (4) is added after soil loading. Two aluminium U-channels (5) linked by a steel wire (6) inserted in the outer nylon mesh (7), make up the frame that closes the rhizobox. (c) Rhizobox support. Twenty-two rhizoboxes are aligned in two rows and separated with white polystyrene sheets. The glass side (anterior) of the rhizobox faces downwards with an inclination of 45°. Pieces of anti-slip mesh are laid in trays holding the rhizoboxes (arrowhead).

Table 1 Root system architecture parameters

Parameter	Unit	Computing method
Total Area	cm^2	Number of pixels detected as root
Convex hull area	cm^2	Area of the smallest convex hull enclosing the root system
Total Length	cm	Number of the pixels of the skeletonized root system
Growth rate	$cm^2\ d^{-1}$	Difference of root system area over unit of time
Depth	cm	Maximal vertical extension
Width	cm	Maximal horizontal extension
Centroid	cm	Coordinates of the centre of mass with respect to the root system
Solidity	N/A	Total root area relative to convex hull area
Density	N/A	Number of root pixels within a defined square region

sides. This experiment was conducted until 35 DAS for 10 rhizoboxes each with posterior compression at inclinations of 30° or 45°, respectively (Figure S4).

Total root area and length were the parameters most affected, with a maximum value for data lost as a result of root growth obscured by soil close to 6% for the total visible area and 9% for the total visible length at 35 DAS with rhizoboxes inclined at 45° (Figure S4a,b). By contrast, for convex hull area and lateral extension (root system width), a maximum underestimate of approximately 2.0 and 3.5%, respectively, was observed at 21 DAS (Figure S4c,d), and root system depth values were unaffected by considering only data from the anterior side (data not shown). RSA parameters were computed separately for each RSA parameter from the anterior side only, and from superimposed data for both sides in order to calculate the fraction of visible data lost, at 30° or 45° inclination, respectively (Figure S4e,f).

Accuracy of computed RSA parameters. To validate the accuracy of our computed data, ground-truth (measured) data were collected by opening the rhizoboxes (grown at inclinations of 30° or 45° with posterior compression) and washing the whole root system at 35 DAS. The computed root depth values understated the measured values by −1.3% (Figure S5a), maximally, and were very closely correlated (R^2 = 0.99; Figure S5b). Images of the washed root system were taken to compute its area (washed root area) and to compare this with the visible (anterior) root area. After drying, dry root mass was also compared with visible root area. Visible root area and dry root mass are better correlated when rhizoboxes are inclined at 45° (R^2 = 0.66), compared with 30° (R^2 = 0.19) (Figure S6a). We then compared the visible root area with the washed root area (Figure S6b). The correlations between visible root area and washed root area were similar at both angles (R^2 = 0.79 and 0.76 for 30° and 45°, respectively), but more roots are visible on the front side at an inclination of 45°.

We then analysed how the anteriorly visible root system related to the washed root system (Figure S6c). The mean values of the visible root system as a fraction of the washed root system do not significantly differ (Student's *t*-test, P = 0.1) between inclinations of 30° and 45°; however, maximal visibility was 74.0 and 85.7% for inclinations of 30° and 45°, respectively. On average, the washed root area tended to be higher at an inclination of 30°, but did not significantly differ from the washed root area at an inclination of 45° (Student's *t*-test, P = 0.06; Figure S6d).

In summary, we concluded that the rhizobox system with soil compressed against the posterior side and inclined at 45°, with the anterior (glass) side facing down, provided the most accurate data on the development of RSA over time.

Root system analysis of two chickpea genotypes

Root system architecture parameters. Images of two chickpea genotypes (Desi ICC1882 and Kabuli ICC8261) grown in rhizoboxes were acquired three times per week

from 10 DAS until 35 DAS at intervals of 2–3 days (Movie S1). The segmented root systems at 5, 12, 19, 26 and 33 DAS for each genotype clearly show visually contrasting root systems (Figure 2a,b). Segmented images were analysed to extract the emergent RSA parameters and plotted over time (Figures 2c,d and S7; Table 1).

The total area of the root system (Figure 2c), computed by counting the number of pixels segmented as 'root' in an image, exhibits a similar curve profile as root system length over time (Figure S7e). The total area was significantly greater for ICC8261 from 26 DAS. The relative root growth rate per area unit (Figure 2d) was computed as the ratio of the difference between the root system area at time t_n and at time $t_{(n-2)}$, over the difference in time (ΔDAS). This growth rate initially increased until 24 and 26 DAS for ICC1882 and ICC8261, respectively, and then decreased. It was significantly greater (Student's *t*-test, $P < 0.05$) for ICC8261 from 19 DAS.

Root system depth (Figure S7a), which corresponds to the vertical position of the deepest root pixel, increases linearly during that time course, with an inflection observed at 30 DAS, reflecting reduced root apical growth. The maximum individual value recorded for that parameter was approximately 1.3 m, confirming that in our system root growth was not restricted in terms of depth. No significant difference was observed between the two genotypes for depth, although ICC8261 tended to have a deeper root system. Root system width (maximal lateral extension, Figure S7b), computed as the horizontal distance between the right- and left-most pixels, also increases, but is likely to be constrained by the rhizobox size from approximately 25 DAS onwards.

The average location of all the root pixels (centroid) was plotted relative to the coordinates of the rhizobox (Figure S7c). On average, the centroid is aligned with the central vertical axis, showing that the root system is distributed equally across the horizontal axis. Convex hull area (Figure S7d) increases during the time course, to reach approximately 2730 and 3500 cm^2 at 35 DAS for ICC1882 and ICC8261, respectively. The differences became significant (Student's *t*-test, $P < 0.05$) from 17 DAS onwards.

The total length of the root system (Figure S7e) was calculated as the number of pixels after segmented images were skeletonized (Giuffrida *et al.*, 2015; Wu *et al.*, 2018); this parameter increased exponentially over time during the experiment, reflecting the increased number of actively growing root tips. Total length was significantly greater for ICC8261 from 21 DAS (Student's *t*-test, $P < 0.05$). Root system solidity (Figure S7f), i.e. the ratio of total root area over the convex hull area, decreased slightly until 12 and 14 DAS for ICC1882 and ICC8261, respectively, then increased. This parameter was significantly greater for ICC8261 from 26 DAS (Student's *t*-test, $P < 0.05$).

Root density maps inform on soil–root interface. We analysed dynamic changes to root distribution by assessing root area in non-overlapping square grids of approximately 3 cm^2 (200 × 200 pixels) across the entire surface of the rhizobox. Root density was analysed separately for each genotype and represented as a heat map (Figures 3 and S8). The temporal progression of growth is plotted as the difference in root pixels for each t_n and $t_{(n-3)}$ (1-week interval) (Figure 3a). This analysis reveals a combination of two growth modes for both genotypes: (i) expansion of total root area to occupy new soil volumes within the existing convex hull; and (ii) root growth that enlarges the convex hull to expand the plant–soil interface. We then analysed root density differences between genotypes (Figure 3b). This analysis reveals that globally, ICC8261 produces a higher root density compared with ICC1882 throughout the convex hull, with only the stratum between 15 and 30 cm of depth showing locally restricted higher densities for ICC1882. Chickpea roots grow more avidly, particularly at 21, 28 and 35 DAS, between 25 and 50 cm in depth, flanking the middle axis defined by the primary root; this is more pronounced for ICC8261 than for ICC1882 (Figure S8), suggesting that this stratum is more intensively exploited for resources.

We then examined root growth activity in approximately 15-cm-deep horizontal strata (Figure 4a,b). From 30 to 90 cm in depth, the root area density is significantly higher for ICC8261 at 35 DAS. When normalized to total root area per genotype, the relative distribution of root area per stratum shows that ICC1882 invested significantly more in root growth between 15 and 30 cm of depth than ICC8261 (Figure 4c). By contrast, ICC8261 exhibits a higher relative proportion of its root system lying between 60 and 90 cm of depth.

Local root senescence in shallow soil strata as root growth in deeper strata progresses

In an independent longer experiment, root area in cultivar ICC8261 was examined per stratum to determine its spatiotemporal progression (Figure S9). From 6 to 34 DAS the root area increased in successively deeper strata (Figure S9a), whereas from 34 to 52 Das the root area gradually declined progressively from shallow to deeper strata (Figure S9b). The decrease in root area was the highest between 30 and 45 cm of depth, but was not visible below 105 cm of depth. This suggests that as the plant exploits progressively deeper strata, the roots in shallower strata die and atrophy as resources have possibly become depleted.

The switch from vegetative to reproductive phase impacts RSA dynamics

To examine the dynamics of RSA parameters after the transition from the vegetative to the reproductive phase of

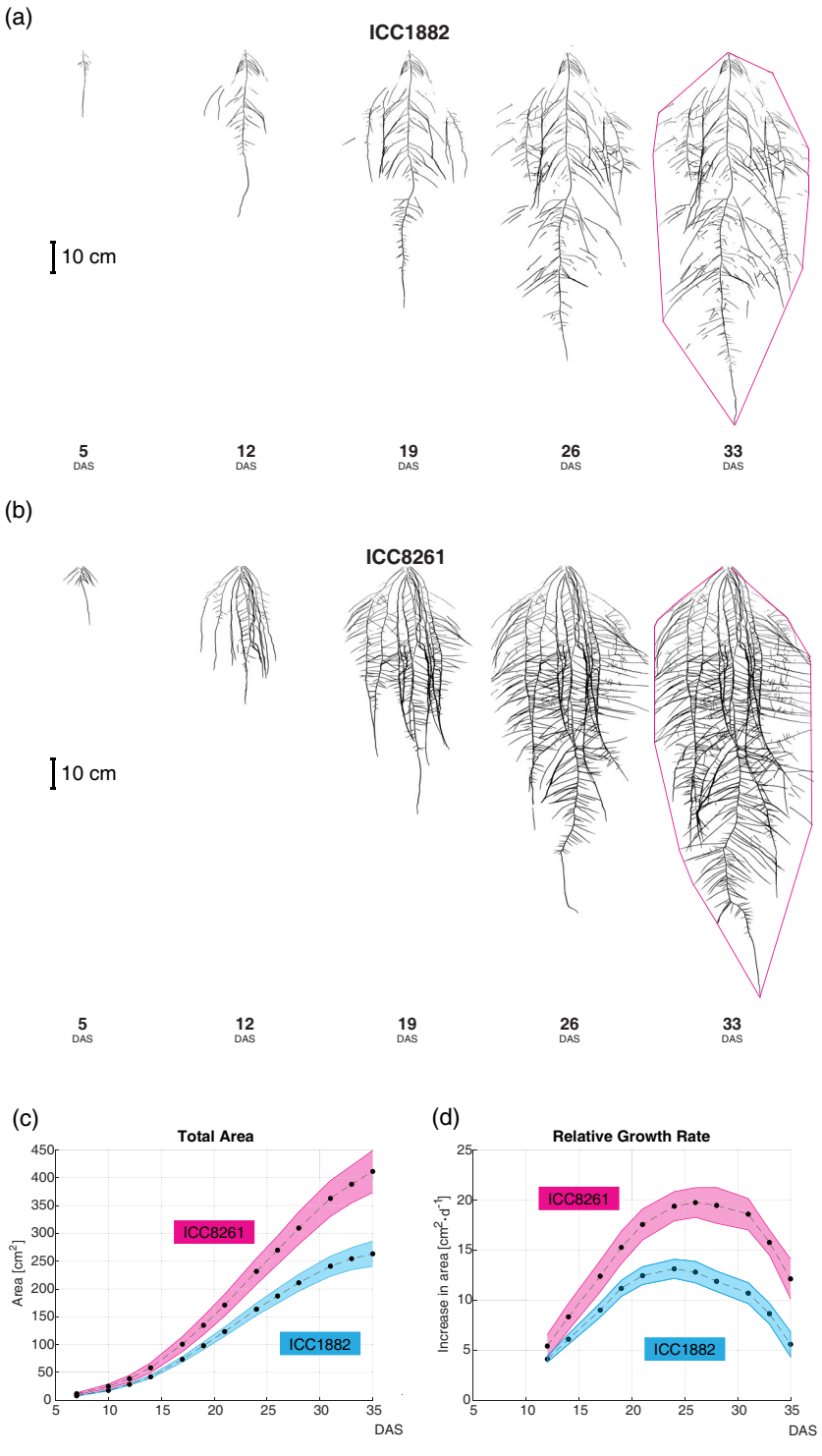

Figure 2. Evolution of root system parameters of two chickpea genotypes in rhizoboxes.
(a&b) Segmented images of the root system in one rhizobox for each genotype at 5, 12, 19, 26 and 33 days after sowing (DAS). (a) ICC1882 and (b) ICC8261. The convex hull corresponding to each time was overlapped on the segmented root system image at 33 DAS (magenta lines).
(c&d) Selected root system parameters (ICC1882 in cyan and ICC8261 in magenta). The points and dashed line show the mean and the shaded region indicates standard error (ICC1882 $n = 9$ and ICC8261 $n = 10$). (c) Total area: summed root pixels. (d) Relative growth rate: difference of root system area at time t_n relative to time t_{n-2} over unit time.

the life cycle, we acquired images of three ICC1882 rhizoboxes until 46 DAS. RSA parameters (root area, root length, root depth and root growth rate) were extracted. Both root area and root length exhibit a characteristic S-shape curve, whereas root depth is more linear for the duration (Figure 5a–c). This time course included two key landmarks of the reproductive phase: the appearance of flower buds (cyan arrow) and the opening of the first flower(s) (magenta arrow), as indicated in Figure 5(a–d, e–g). Interestingly, those two key stages of the reproductive phase coincide with changes in root growth rate dynamics. Root growth rate peaked at bud appearance (30 DAS;

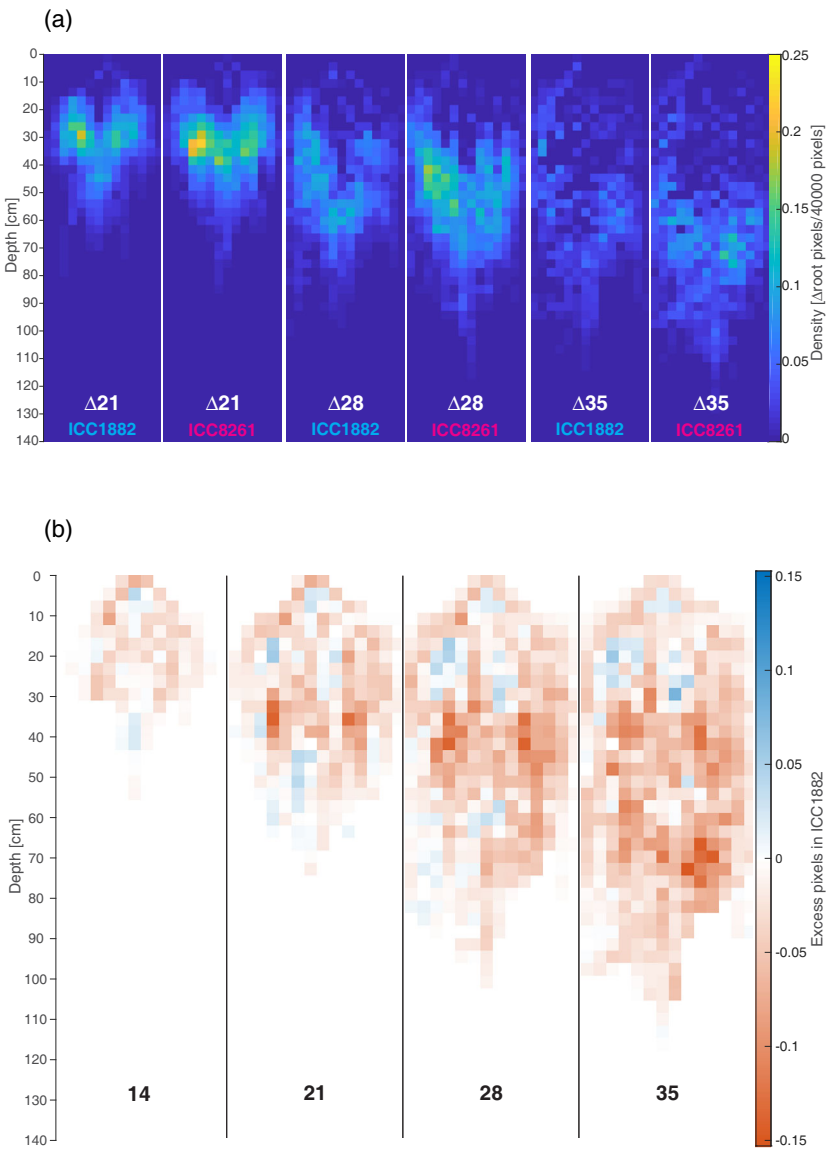

Figure 3. Average root area density for two chickpea genotypes in rhizoboxes over time. Computed in a grid of 200 × 200 pixel squares covering the whole rhizobox and the mean taken from several rhizoboxes (ICC1882 $n = 9$ and ICC8261 $n = 10$). Panels show data from 21, 28 & 35 days after sowing (das). The scale unit corresponds to the number of root pixels per square.
(a) Time relative root density. This was computed as the difference in average number of root pixels between time t_n and time t_{n-3} (one week interval), over the difference in time (Δ das).
(b) Difference in average root density between genotypes. This was computed as the difference in average number of root pixels between genotypes ICC1882 and ICC8261. Therefore, a positive number (blue) indicates a comparatively greater root density of ICC1882 while a negative number (red) indicates a greater root density of ICC8261.

Figure 5d) then gradually decreased until the first flower(s) opened (37 DAS; Figure 5d), after which the decline in growth rate accelerated.

Comparability across different species and sites

To evaluate the utility of the rhizobox system for other plants, particularly monocot crop species, we also tested the growth of barley. Barley (var. Concerto) was grown in rhizoboxes and the root system was imaged repeatedly until 25 DAS (Figures S10 and S11). The detection of barley roots was as robust as for chickpea, although some thinner lateral roots were not always detected. Monocot root systems often exhibit thinner secondary or tertiary roots that challenge the segmentation process established for chickpea. Most RSA parameters (width, length, area and convex hull area) increased exponentially in barley, whereas root growth rate and depth increased linearly (Figure S10). In contrast to chickpea, root solidity in barley decreased continuously, indicating that convex hull area increases faster than root area. When analysing local root densities, the growth activity of the root system until 25 DAS revealed that in Concerto, early root system development focused on accessing deeper soil strata, although this result may have been biased by the incomplete detection of lateral roots (Figure S11b).

The rhizobox system was co-developed in Edinburgh (UK) and in Debre Zeit (Ethiopia). As the majority of chickpea field cultivation in Ethiopia is conducted in vertisols, a unique and clay-rich soil, we tested whether rhizoboxes would support chickpea growth and allow root system visualization when filled with vertisol. When loaded with vertisol from local farmland, the rhizoboxes supported

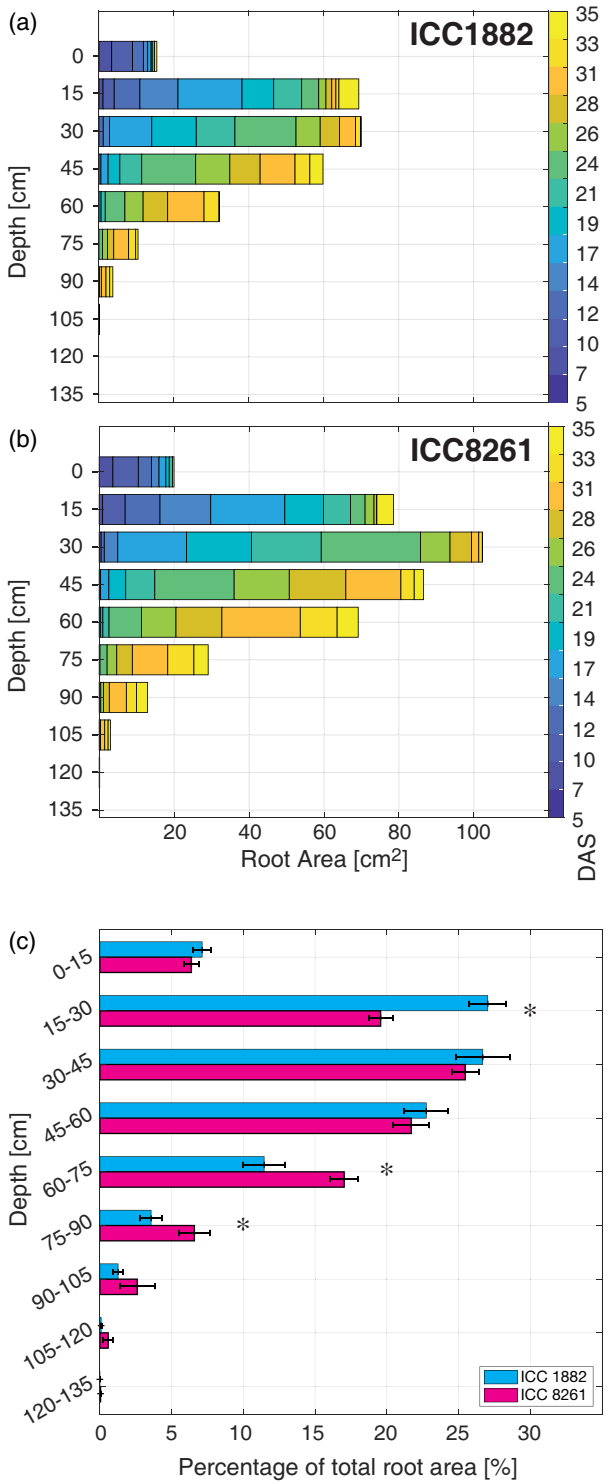

Figure 4. Average root area of two chickpea genotypes.
(a&b) Root area at different depths in rhizoboxes over time.
(a) ICC1882 (b) ICC8261. Coloured scale indicates days after sowing (DAS).
(c) Percentage of total root area at different depths at 35 DAS (ICC1882 in cyan and ICC8261 in magenta). Calculated in 15 cm deep horizontal sections and using the mean taken from several rhizoboxes. Asterisks indicate a significant difference between the root area of the genotypes at 35 DAS at the specified depth (DAS -Tukey $P < 0.05$, ICC1882 $n = 9$ or ICC8261 $n = 10$).

chickpea growth and RSA parameters could be analysed successfully (Figure S12a–h). Data from two local cultivars are presented here: images from rhizoboxes growing 'Natoli' and 'Fetenech' cultivars were successfully stitched (Figure S12a,b, respectively), and their analysis reveals distinct growth behaviour (Figure S12c–h).

DISCUSSION

We developed a growth (rhizobox) and imaging system using low-cost commodity components to study root development in soil, frequently and non-destructively, during the plant life cycle. The system is based on frugal engineering principles and can be operated without extensive training. It can therefore be assembled and operated in most low- and middle-income countries. We routinely used this system to capture RSA parameters for chickpea and barley. Low-cost commodity components and the features of the data acquisition and processing pipeline will now enable this powerful tool to be used by breeders in many countries to inform their strategies for enhancing crop performance.

Growth system validation

To reflect genetically encoded (genotype) and adaptive (environment) root growth behaviours with higher fidelity, and generate outcomes informative for breeders, we focused on characterizing soil-grown roots (Figure 1). For example, a recent study characterizing the root systems of 270 chickpea genotypes in a semi-hydroponic system (Chen *et al.*, 2017) showed that varieties exhibiting short root systems in soil (e.g. ICC283 and ICC1882; Kashiwagi *et al.*, 2005) display intermediate or deep root systems in semi-hydroponic growth. Hence, root phenotyping systems not based on soil have diminished predictive value for breeders: in those conditions, roots do not face soil physical constraints, experience a different hydrology and nutrient distribution, and do not interact with the microbiome, all factors to which root systems are known to respond. We conclude that soil-based growth systems reflect root behaviour in natural conditions with higher fidelity, and therefore are of greater value to breeders.

Rhizobox-type soil-filled systems with one transparent side for root system visualization have been developed previously (e.g. Sachs, 1865; Price *et al.*, 2002; Devienne-Barret *et al.*, 2006; Bodner *et al.*, 2017). These systems differ in their dimensions, and hence in the volume of soil available for root system growth. Small growth systems with extremely thin soil layers that can be readily handled have been reported, but these are too small to support unimpeded root growth throughout the life cycle of most crops (Rellan-Alvarez *et al.*, 2015). Thicker soil layers or double-glass large rhizoboxes make regular manual handling challenging, however, and also considerably increase the costs, thereby reducing the ability to process large

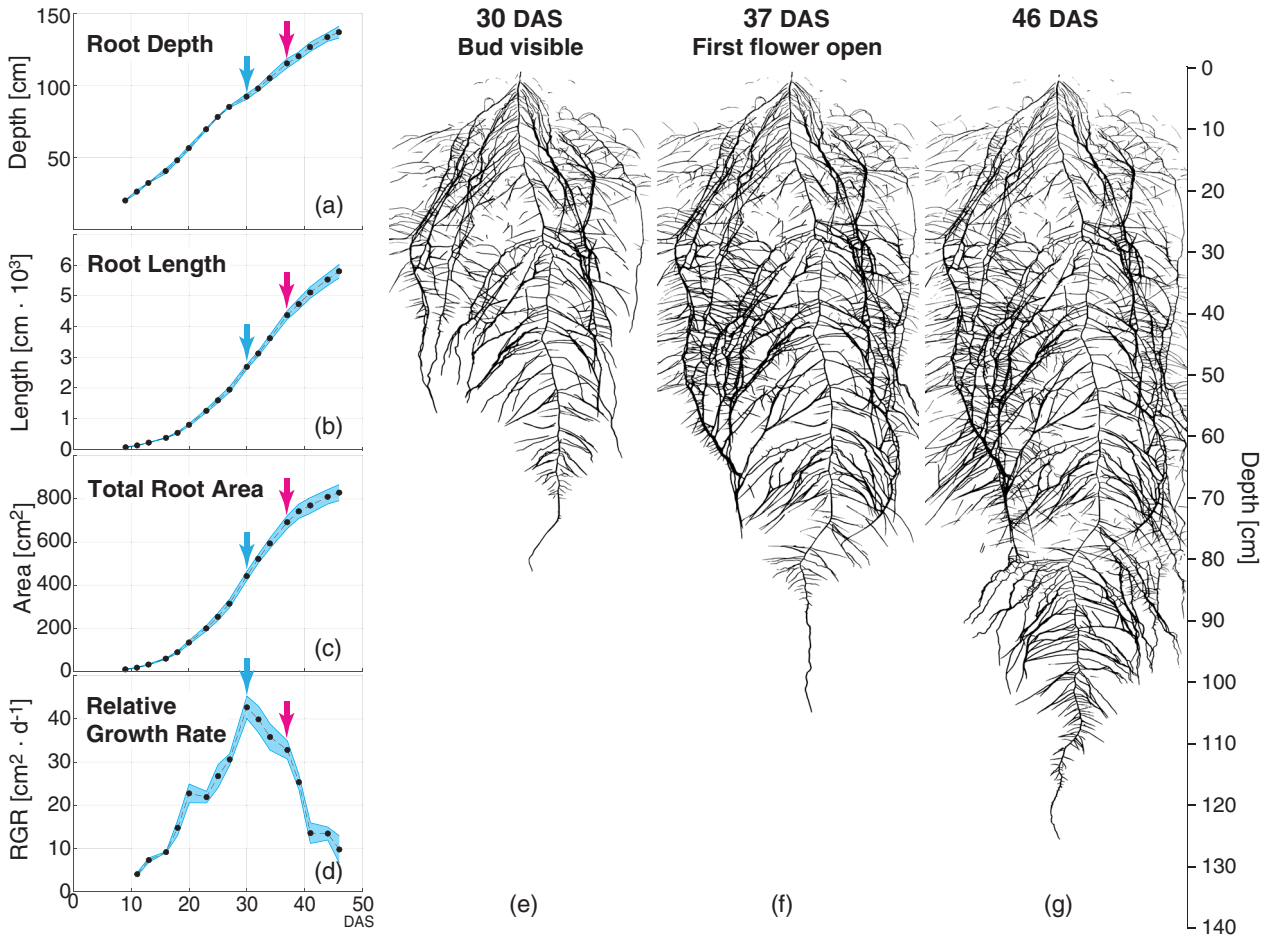

Figure 5. Impact of the switch to reproductive phase on chickpea root system parameters in a rhizobox.
(a–d) Root system parameters analysed for the chickpea genotype ICC 1882. The green arrow shows the time of emergence of the first bud and the purple arrow shows the time of the first flower open. Points show the mean and bars show standard error (n = 3). (a) Root depth (b) Root length (c) Root area (d) Relative growth rate (RGR) (e) Segmented images of one root system of the chickpea genotype ICC 1882 in rhizobox at 30 (first bud visible), 37 (first flower open) and 46 days after sowing (DAS).

numbers of rhizoboxes and the overall throughput is reduced. The rhizobox system reported here strikes a balance between large overall dimensions, which impose few constraints on root architectural development, and ease-of-handling requirements and low costs.

For the maximum visualization of roots, their gravitropism is usually exploited by inclining the growth box at angles of between 15° and 45° from the vertical. We aimed to maximize the fraction of the root system visible on the imaged front glass side. Double-glass rhizoboxes were used to assess how inclination angle and direction of soil compression affect the root system fraction visible on the front side. The soil layer in the rhizoboxes described here is relatively thin (6 mm) compared with other systems (e.g. Nagel *et al.*, 2012; Jin *et al.*, 2015); however, over time an increasing fraction of the root system will be hidden within the soil or will grow against the back side. The latter will only be seen in double-glass rhizoboxes, and the former only after the invasive removal of the soil matrix. This 'invisible' fraction of the chickpea root system mainly affected root area and length, but had little influence on convex hull area and width (Figures S3–S6). Interestingly, this never affected the depth calculation for chickpea roots, because the primary root tip was always visible. Soil compression against the posterior side combined with an inclination of 45° was optimal to maximize root system visibility on the anterior (normally imaged) side (Figure S3). An average of 75.4% and a maximum of 86.2% of the visible root system was imaged on this side. When compared with a previous study (Nagel *et al.*, 2012), where the length of the root system imaged on the transparent side was compared with the length of the entire root system after soil removal, our system performed similarly to their best results: Nagel *et al.* (2012) report species-dependant differences in anterior visibility, ranging from 17% for *Zea mays* to 77% for *A. thaliana*. Moreover, a comparison of our system (6-mm soil thickness) with one containing more soil (34-mm soil thickness) shows that a phylogenetically close

relative to chickpea, *Vicia faba* (faba bean), does not perform markedly better with approximately six times more soil to exploit (Belachew *et al.*, 2018).

We conclude that our affordable growth and imaging system yields results as relevant as those obtained with substantially more expensive and complex systems: for example, automatic root phenotyping platforms (Nagel *et al.*, 2012; Belachew *et al.*, 2018).

Robustness of analysis and significance of parameters

In any soil-based system analysed by visible wavelength imaging, some root parameters (e.g. topological parameters such as the number of secondary roots or lateral root density) are incompletely captured because of gaps caused by the soil obscuring parts of or entire roots. By contrast, root system analysis (e.g. architectural parameters such as convex hull area or root system length) is more tolerant to uncertainty and noise, as not every root or its contiguity must be identified for meaningful information to be obtained. Topological analysis is limited by hidden parts of the root system, resulting in discontinuous root topology. Nonetheless, a promising recent approach has demonstrated that such hidden root parts can be recovered with the use of deep neural networks (Chen *et al.*, 2019).

The focus on RSA parameters in the analysis of rhizobox images allowed us to develop algorithms to automatically extract parameters (e.g. convex hull area and root density) with direct utility for: (i) describing fundamental mechanisms in plant root biology; and (ii) local breeders to improve the efficacy of crop selection. RSA parameters reflect soil resource acquisition strategies: root system length and area describe the individual investment in root biomass for resource foraging and acquisition. During the vegetative phase, the continuous increase of the root system that we observed for chickpea (Figures 2 and 5) is commonly reported for other plant species grown in soil-filled systems (Price *et al.*, 2002; Devienne-Barret *et al.*, 2006; Leitner *et al.*, 2014; Yuan *et al.*, 2016). Careful analysis of stratified root area density over time allowed us to identify a shift of resource acquisition capacity towards deeper strata, as dense networks in shallower strata were progressively thinned as the density increased in deeper strata (Figure S9).

To our knowledge only one study has previously described the impact of the switch to the reproductive phase on root growth dynamics, but used destructive sampling (Koelewijn, 2004). Our rhizobox system allowed us to capture images until 7 weeks after chickpea seed sowing, including a part of the reproductive stage, without disturbing root growth. In our system, bud appearance slowed down root growth, with a further decrease after the first flower opens. These dynamics indicate that the plant reduces its investment into root growth, possibly because immobile resources within the densely rooted volume are depleted, or as a result of a shift in resource and metabolic priorities with the onset of reproduction (Koelewijn, 2004). Root growth during the reproductive stage is an underevaluated trait because of the previous lack of suitable experimental approaches for non-destructive data acquisition. It is a relevant trait for breeding for sustainability in arid agriculture, as water uptake is crucial for pod-filling (see review by Vadez *et al.*, 2014).

Root solidity (ratio root/convex hull areas) reflects a trade-off between foraging and space exploration. It provides insight into the strategy to acquire soil resources: expand the perimeter of the system or intensify, with higher solidity reflecting more intense resource foraging, within the perimeter of the explored area. Solidity in the chickpea genotypes tested shows a slight decreasing trend until 10 and 14 DAS for ICC8261 and ICC1882, respectively (Figure S7f), implying that convex hull area (i.e. the explored area) increases faster than root system area. Resource foraging then becomes more intense until 35 DAS, as solidity increases.

Interestingly, the initial study of barley RSA revealed a resource acquisition strategy that differed from chickpea (Figures S10 and S11). The barley root system grows more extensively (predominantly in depth) rather than intensively, leading to a continuous decrease in solidity over the sample time (Figure S10). Consistent with this, the highest root growth activity is regularly close to the deepest root tips (Figure S11b). Our rhizobox system allows for interspecies comparisons, which are relevant ecologically, and for the development of novel multi-species or multicultivar cropping systems aimed at minimising competition for resource acquisition within a given environment (Li *et al.*, 2014; Wang *et al.*, 2014; Weiner *et al.*, 2017). Studies are in progress in our group using these tools to examine the responses of different crops and cultivars to limiting mobile resources (e.g. water and nitrogen), immobile resources (e.g. phosphate and iron), interactions with the soil microbiota, and associated changes to metabolism and physiology.

Informing chickpea breeding in low- and middle-income countries

Previous studies with chickpea roots were focused on root parameters acquired by destructive experiments and were limited to a few time points of the life cycle (Krishnamurthy *et al.*, 1998; Serraj *et al.*, 2004; Ali *et al.*, 2005; Kashiwagi *et al.*, 2005, 2006; Pang *et al.*, 2011; Purushothaman *et al.*, 2017; Pang *et al.*, 2018). In contrast, the rhizobox system reported here permits repeated data acquisition and thus permits continuous analysis of root system parameters dynamically and non-destructively. The latter is a key feature for the utility of this system: for example, drought conditions are thought to be particularly damaging around the time of onset of flowering. Therefore, the ability to analyse

root system architectural parameters over time is crucial to identify germplasm that directs rapid, early and deep root growth to access residual moisture (Gaur *et al.*, 2008; Upadhyaya *et al.*, 2012). Our observations have highlighted significant differences in numerous RSA parameters between two chickpea varieties, which reflect different resource foraging capacities: ICC1882 and ICC8261 invested more roots in upper and lower soil strata, respectively (Figures 3b and 4). Those results are consistent with previous studies describing the Desi ICC1882 and Kabuli ICC8261 cultivars as contrasting in terms of root system (Kashiwagi *et al.*, 2005).

This rhizobox system is currently being established and tested at the Ethiopian Institute of Agricultural Research (EIAR) at Debre Zeit (Bishoftu) in Ethiopia. Initial results (Figure S12) indicate that the system can be used with local vertisols, which are among the most challenging soils for agriculture because of their rheological properties (Jones *et al.*, 2013).

We conclude that the newly developed rhizobox system based on commodity components and powerful analytical tools will be useful to inform local breeders to address food security challenges by accelerating the enhancement of RSA-based traits associated with increased resilience and resource acquisition. The system also has great potential to study new approaches to optimize cropping practice, for example to optimize plant spacing to balance below ground competition with yield and to study fundamental questions such as source-sink relationships and resource allocation between different plant organs.

MATERIALS AND METHODS

More detailed Materials and Methods are provided in Data S1.

Rhizobox design and construction

The rhizobox (Figure 1a,b), made of the components described in Table S1, holds a 6 mm layer of soil between a sheet of polyvinylchloride (PVC; 1500 mm × 450 mm × 6 mm), a 6 mm silicone spacer, and a glass pane of the same dimensions as the PVC backing for a total soil volume of approximately 3.7 dm^3. The assembly is held together by two aluminium U-channels on the sides, and a wire inserted into a folded piece of nylon mesh to close the bottom of the rhizobox.

After preparation, the soil is manually spread uniformly, then compressed to ensure that the surface is level with the silicon strips. After adding the glass pane, the system is closed with the U-channel frame described above.

Plant material and growth conditions

In Edinburgh, chickpea (*Cicer arietinum* L.) seeds were prepared then sown in soil substrate for 2–3 days before transplanting the seedling into a rhizobox. In Ethiopia, chickpea seed were imbibed and sown into pots filled with local vertisol, then transferred into rhizoboxes after 7 days. Barley (*Hordeum vulgare* L., variety *Concerto*, SRUC, UK) seeds were directly sown at the top of the rhizobox for *in-situ* germination. Plants were grown in rhizoboxes in a glasshouse at the King's Building campus (Edinburgh, UK, 55°55′14.9″N, 3°10′09.9″W) and at the Debre Zeit Agricultural Research Centre, (Debre Zeit/Bishoftu, Ethiopia, 8°46′10.4″N, 38°59′55.6″E). Rhizoboxes were supported at an angle of 45° by metallic supports (Figure 1c), built using components described in Table S2. Rhizoboxes were placed in trays covered with anti-slip mesh. White polystyrene blocks were used as spacers between the support and rhizoboxes. The whole system was wrapped with white-black sheeting to insulate against excessive radiative heating. Water was added to the trays at the base of the system and maintained to ensure a constant supply. The glasshouse day and night temperature setpoints were 26 and 16°C, respectively.

Imaging station

An imaging station for rhizoboxes was built (Figure S1) using components described in Table S3. The rhizobox is illuminated from the interior of the imaging station. An aluminium U-channel, parallel and medial to the rhizobox, supports the cameras. Five cameras were spaced 30 cm apart to ensure enough overlap between images for further stitching. The distance between lens and rhizobox was set at 78 cm. The imaging station was isolated from daylight using a black felt layer.

Camera and image capture

We used the affordable imaging hardware and software platform Phenotiki (Minervini *et al.*, 2017), after adapting it for this project to use adjustable focus camera sensors (Raspberry Pi Camera) for imaging. The Phenotiki sensor software was modified to trigger five cameras simultaneously by using a master-slave model, where one Raspberry Pi (the master device, configured with the extended Phenotiki Sensor Software) allows the other acquisition devices (the slaves) to connect *via* wireless communication. To acquire images, the master triggers and collects the images obtained from all devices and stores them locally. The user can operate the sensor *via* a web-based interface. To reduce overhead during image acquisition, images were uploaded into cloud-based storage (Google Drive) at scheduled times of the day (pipeline in Figure S2). Alternatively, in case of suboptimal connectivity, the user can also download the acquired images directly from the Phenotiki interface. Acquisition parameters (see Table S4) are the same for each device. Cameras are placed and configured in the imaging station. To compensate for lens distortion, camera calibration was performed (Zhang, 2000), using a chessboard of ArUco markers (typically referred as ChAruco) to determine the intrinsic camera parameters (Zhang, 2000; Romero-Ramirez *et al.*, 2018). A series of permanent ArUco markers (4 cm^2) were fixed to the interior of the imaging station frame that flanks the aperture for the rhizobox to be visible by the cameras and further improve picture assembly. Images generated using one exposure were of sufficient quality across the horizontal extent of the rhizobox. Combining images from up to 5 different exposure settings in a 'high dynamic range' (HDR) mode is also possible, but comes at the cost of increased computational load and storage requirements.

Image processing for stitching

Following image acquisition, image series of one rhizobox are processed to create a large mosaic stitching to obtain a single large image of the rhizobox (akin to the process of creating a panoramic image from multiple images). QR codes placed on the top corners of the glass pane on each rhizobox are decoded automatically from the stitched images to identify them.

Image segmentation

The stitched, large, image was used to segment the root system from soil background. Segmentation is performed in two steps: (i) Foreground-Background (FG-BG) segmentation; and (ii) noise removal. *FG-BG segmentation*. Imaging effects and artefacts preclude the use of a simple thresholding operation to separate root from soil. Therefore, we analysed the root images row by row to identify root pixels, which includes a parabolic threshold function to compensate for lateral illumination. *Noise removal*. Although the previous step is able to determine the plant roots, over-segmentation can still occur, due to clutter in the scene (*e.g.* presence of droplets inside the rhizobox). To alleviate this, we perform a refining step to remove the noise. Once the segmentation of the RSA is obtained, root traits are extracted as reported in Table 1. After the data were extracted from the segmentation mask, they were converted from pixels into cm. See Data S1 and Figure S13 for more details.

Local root density

To determine local root density the segmented image of a root system is sub-divided into a regular grid, where each cell is 200 × 200 pixels (ca. 9 cm^2). For each cell, we compute the total number of root pixels from the segmentation mask and convert the measure to cm^2. For dynamic analyses, we compute the difference of two consecutive root densities at time t_n and t_{n-1}.

ACKNOWLEDGEMENTS

The authors thank Joanna Jones and Şeyhmus Dündar for testing some initial rhizobox designs, Sam Anderson and Javier Surís Auguet for help with soil preparation and building in glasshouse, Peter Hoebe from Scotland's Rural College (SRUC) for providing barley seeds. PD thanks BBSRC (BB IAA 15/16–PD & BB GC IAA 16/17) for funding which supported early-stage work with rhizoboxes. ST and PD thank BBSRC for funding (BB/P023487/1). CC thanks CONICYT PFCHA/DOCTORADO BECAS CHILE/2016 – 72170128 for a PhD scholarship. This research was carried out with resources provided by the Edinburgh Plant Growth Facility, a specialist service provider for plant growth at the University of Edinburgh.

AUTHOR CONTRIBUTIONS

All authors contributed to the development of the rhizobox growth system for visualising root growth, VG and ST developed and implemented image capture and data processing, TB, CC and IR developed the growth conditions for chickpea growth in rhizoboxes. TB, CC, VG, IR, ST and PD wrote the paper.

CONFLICTS OF INTEREST

The authors declare no conflicts of interest.

DATA AVAILABILITY STATEMENT

Software, test data for its evaluation and CAD files to construct rhizoboxes have been made available at: https://doi.org/10.7488/ds/2841. Data and code implementing the analysis pipeline is available on request by emailing the senior/co-corresponding authors.

SUPPORTING INFORMATION

Additional Supporting Information may be found in the online version of this article.

Figure S1. Imaging station for imaging of a rhizobox.

Figure S2. Diagram of image capture and processing pipeline.

Figure S3. Evaluation of root system growth with double-glass rhizoboxes.

Figure S4. Relative underestimation of computed parameters at different rhizobox angles and over time.

Figure S5. Comparison of computed with measured (ground truth, GT) values.

Figure S6. Correlation between anterior root area, root dry mass and washed root area at different rhizobox angles.

Figure S7. Evolution of root system parameters of two chickpea genotypes in rhizoboxes.

Figure S8. Average root area density for two chickpea genotypes in rhizoboxes.

Figure S9. Spatio-temporal evolution of root area in the rhizobox.

Figure S10. Evolution of root system architecture parameters of a barley (*Hordeum vulgare*, var. Concerto) in rhizobox.

Figure S11. Root area density analysis of a barley (*Hordeum vulgare*, var. Concerto) in rhizobox.

Figure S12. Evolution of root system parameters of two chickpea genotypes in rhizoboxes in Ethiopia.

Figure S13. Root segmentation algorithm.

Table S1. List of rhizobox components.

Table S2. List of rhizobox support components.

Table S3. List of imaging station components.

Table S4. Parameters for Phenotiki Sensor Setup.

Data S1. Materials and methods.

Movie S1. Time-lapse development of root system in a rhizobox.

OPEN RESEARCH BADGES

This article has earned Open Data and Open Materials badges. Data and materials are available at http://chickpearoots.org/resourcesandlinks; https://doi.org/10.7488/ds/2841.

REFERENCES

Ali, M.Y., Johansen, C., Krishnamurthy, L. and Hamid, A. (2005) Genotypic variation in root systems of chickpea (*Cicer arietinum* L.) across environments. *J. Agron. Crop. Sci.* **191**, 464–472.

Atkinson, J.A., Rasmussen, A., Traini, R., Voss, U., Sturrock, C., Mooney, S.J., Wells, D.M. and Bennett, M.J. (2014) Branching out in roots: uncovering form, function, and regulation. *Plant Physiol.* **166**, 538–550.

Avramova, V., Nagel, K.A., AbdElgawad, H., Bustos, D., DuPlessis, M., Fiorani, F. and Beemster, G.T.S. (2016) Screening for drought tolerance of maize hybrids by multi-scale analysis of root and shoot traits at the seedling stage. *J. Exp. Bot.* **67**, 2453–2466.

Belachew, K.Y., Nagel, K.A., Fiorani, F. and Stoddard, F.L. (2018) Diversity in root growth responses to moisture deficit in young faba bean (*Vicia faba* L.) plants. *PeerJ*, **6**, e4401.

Bodner, G., Alsalem, M., Nakhforoosh, A., Arnold, T. and Leitner, D. (2017) RGB and spectral root imaging for plant phenotyping and physiological research: experimental setup and imaging protocols. *J. Vis. Exp.* **126**, e56251. https://doi.org/10.3791/56251

Bouma, T., Nielsen, K., Van Hal, J. and Koustaal, B. (2001) Root system topology and diameter distribution of species from habitats differing in inundation frequency. *Funct. Ecol.* **15**, 360–369.

Burridge, J.D., Jochua, C.N., Bucksch, A. and Lynch, J.P. (2016) Legume shovelomics: High—Throughput phenotyping of common bean (*Phaseolus vulgaris* L.) and cowpea (*Vigna unguiculata* subsp, *unguiculata*) root architecture in the field. *Field. Crop. Res.* **192**, 21–32.

Burridge, J.D., Schneider, H.M., Huynh, B.L., Roberts, P.A., Bucksch, A. and Lynch, J.P. (2017) Genome-wide association mapping and agronomic impact of cowpea root architecture. *Theor. Appl. Genet.* **130**, 419–431.

Chen, H., Giuffrida, M.V., Doerner, P. and Tsaftaris, S. (2019) Blind inpainting of large-scale masks of thin structures with adversarial and reinforcement learning. *arXiv*, **2019**, 1–11. arXiv: 1912.02470.

Chen, Y., Ghanem, M.E. and Siddique, K.H. (2017) Characterising root trait variability in chickpea (*Cicer arietinum* L.) germplasm. *J. Exp. Bot.* **68**, 1987–1999.

de Dorlodot, S., Forster, B., Pages, L., Price, A., Tuberosa, R. and Draye, X. (2007) Root system architecture: opportunities and constraints for genetic improvement of crops. *Trends Plant Sci.* **12**, 474–481.

Devienne-Barret, F., Richard-Molard, C., Chelle, M., Maury, O. and Ney, B. (2006) Ara-rhizotron: an effective culture system to study simultaneously root and shoot development of Arabidopsis. *Plant Soil*, **280**, 253–266.

Downie, H., Holden, N., Otten, W., Spiers, A.J., Valentine, T.A. and Dupuy, L.X. (2012) Transparent soil for imaging the rhizosphere. *PLoS One*, **7**, e44276.

Dresbøll, D., Thorup-Kristensen, K., Mckenzie, B., Dupuy, L. and Bengough, A. (2013) Timelapse scanning reveals spatial variation in tomato (*Solanum lycopersicum* L.) root elongation rates during partial waterlogging. *Plant Soil*, **369**, 467–477.

Durand, M., Porcheron, B., Hennion, N., Maurousset, L., Lemoine, R. and Pourtau, N. (2016) Water deficit enhances C export to the roots in *Arabidopsis thaliana* plants with contribution of sucrose transporters in both shoot and roots. *Plant Physiol.* **170**, 1460–1479.

Gaur, P.M., Krishnamurthy, L. and Kashiwagi, J. (2008) Improving drought-avoidance root traits in chickpea (*Cicer arietinum* L.) – Current status of research at ICRISAT. *Plant Prod. Sci.* **11**, 3–11.

Giehl, R.F. and von Wiren, N. (2014) Root nutrient foraging. *Plant Physiol.* **166**, 509–517.

Giuffrida, M.V., Minervini, M. and Tsaftaris, S. (2015) Learning to count leaves in rosette plants. In *Computer Vision Problems in Plant Phenotyping* (Tsaftaris, S.A., Scharr, H. and Pridmore, T., eds). Swansea: BMVA Press, pp. 1.1–1.13.

Heeraman, D., Hopmans, J. and Clausnitzer, V. (1997) Three dimensional imaging of plant roots in situ with x-ray computed tomography. *Plant Soil*, **198**, 167–179.

Iyer-Pascuzzi, A.S., Symonova, O., Mileyko, Y., Hao, Y., Belcher, H., Harer, J., Weitz, J.S. and Benfey, P.N. (2010) Imaging and analysis platform for automatic phenotyping and trait ranking of plant root systems. *Plant Physiol.* **152**, 1148–1157.

Jin, K., Shen, J., Ashton, R., White, R., Dodd, I., Parry, M. and Whalley, W. (2015) Wheat root growth responses to horizontal stratification of fertiliser in a water-limited environment. *Plant Soil*, **386**, 77–88.

Jones, A., Breuning-Madsen, H., Brossard, M. *et al.* (2013) Soil Atlas of Africa Luxembourg: European Commission, Publications Office of the European Union. 176 pp. ISBN 978-92-79-26715-4, https://doi.org/10.2788/52319

Kashiwagi, J., Krishnamurthy, L., Crouch, J.H. and Serraj, R. (2006) Variability of root length density and its contributions to seed yield in chickpea (*Cicer arietinum* L.) under terminal drought stress. *Field. Crop. Res.* **95**, 171–181.

Kashiwagi, J., Krishnamurthy, L., Upadhyaya, H.D., Krishna, H., Chandra, S., Vadez, V. and Serraj, R. (2005) Genetic variability of drought-avoidance root traits in the mini-core germplasm collection of chickpea (*Cicer arietinum* L.). *Euphytica*, **146**, 213–222.

Koelewijn, H.P. (2004) Rapid change in relative growth rate between the vegetative and reproductive stage of the life cycle in *Plantago coronopus*. *New Phytol.* **163**, 67–76.

Krishnamurthy, L., Ito, O., Johansen, C. and Saxena, N.P. (1998) Length to weight ratio of chickpea roots under progressively receding soil moisture conditions in a Vertisol. *Field. Crop. Res.* **58**, 177–185.

Kuijken, R.C., van Eeuwijk, F.A., Marcelis, L.F. and Bouwmeester, H.J. (2015) Root phenotyping: from component trait in the lab to breeding. *J. Exp. Bot.* **66**, 5389–5401.

Kutschera, L. and Lichtenegger, E. (1997) Bewurzelung von Pflanzen in Verschiedenen Lebensräumen. *Stapfia*, **49**, 5–333.

Kutschera, U. (2015) 150 years of an integrative plant physiology. *Nat Plants*, **1**, 15131.

Leitner, D., Felderer, B., Vontobel, P. and Schnepf, A. (2014) Recovering root system traits using image analysis exemplified by two-dimensional neutron radiography images of lupine. *Plant Physiol.* **164**, 24–35.

Li, L., Tilman, D., Lambers, H. and Zhang, F.-S. (2014) Plant diversity and overyielding: insights from belowground facilitation of intercropping in agriculture. *New Phytol.* **203**(1), 63–69.

Lobet, G., Pagès, L. and Draye, X. (2011) A novel image-analysis toolbox enabling quantitative analysis of root system architecture. *Plant Physiol.* **157**, 29–39.

Lynch, J. (1995) Root architecture and plant productivity. *Plant Physiol.* **109**, 7–13.

Lynch, J.P. (2007) Roots of the second green revolution. *Aust. J. Bot.* **55**, 493–512.

Mathieu, L., Lobet, G., Tocquin, P. and Perilleux, C. (2015) "Rhizoponics": a novel hydroponic rhizotron for root system analyses on mature *Arabidopsis thaliana* plants. *Plant Methods*, **11**, 3.

Minervini, M., Giuffrida, M.V., Perata, P. and Tsaftaris, S.A. (2017) Phenotiki: an open software and hardware platform for affordable and easy image-based phenotyping of rosette-shaped plants. *Plant J.* **90**, 204–216.

Morris, E.C., Griffiths, M., Golebiowska, A. *et al.* (2017) Shaping 3D root system architecture. *Curr. Biol.* **27**, R919–R930.

Morris, J.L., Puttick, M.N., Clark, J.W., Edwards, D., Kenrick, P., Pressel, S., Wellman, C.H., Yang, Z.H., Schneider, H. and Donoghue, P.C.J. (2018) The timescale of early land plant evolution. *Proc. Natl. Acad. Sci. USA*, **115**, E2274–E2283.

Naeem, A., French, A.P., Wells, D.M. and Pridmore, T.P. (2011) High-throughput feature counting and measurement of roots. *Bioinformatics*, **27**, 1337–1338.

Nagel, K., Putz, A., Gilmer, F. *et al.* (2012) GROWSCREEN-Rhizo is a novel phenotyping robot enabling simultaneous measurements of root and shoot growth for plants grown in soil-filled rhizotrons. *Funct. Plant Biol.* **39**, 891–904.

Neumann, G., George, T.S. and Plassard, C. (2009) Strategies and methods for studying the rhizosphere-the plant science toolbox. *Plant Soil*, **321**, 431–456.

Padilla, F.M., Mommer, L., de Caluwe, H., Smit-Tiekstra, A.E., Wagemaker, C.A., Ouborg, N.J. and de Kroon, H. (2013) Early root overproduction not triggered by nutrients decisive for competitive success belowground. *PLoS One*, **8**, e55805.

Pages, L. (2016) Branching patterns of root systems: comparison of monocotyledonous and dicotyledonous species. *Ann. Bot.* **118**, 1337–1346.

Pang, J.Y., Yang, J.Y., Ward, P., Siddique, K.H.M., Lambers, H., Tibbett, M. and Ryan, M. (2011) Contrasting responses to drought stress in herbaceous perennial legumes. *Plant Soil*, **348**, 299–314.

Pang, J.Y., Zhao, H.X., Bansal, R., Bohuon, E., Lambers, H., Ryan, M.H. and Siddique, K.H.M. (2018) Leaf transpiration plays a role in phosphorus acquisition among a large set of chickpea genotypes. *Plant Cell Environ.* **41**, 2069–2079.

Pound, M.P., French, A.P., Atkinson, J.A., Wells, D.M., Bennett, M.J. and Pridmore, T. (2013) RootNav: navigating images of complex root architectures. *Plant Physiol.* **162**, 1802–1814.

Price, A.H., Steele, K.A., Moore, B.J. and Jones, R.G.W. (2002) Upland rice grown in soil-filled chambers and exposed to contrasting water-deficit regimes II. Mapping quantitative trait loci for root morphology and distribution. *Field. Crop. Res.* **76**, 25–43.

Purushothaman, R., Krishnamurthy, L., Upadhyaya, H.D., Vadez, V. and Varshney, R.K. (2017) Root traits confer grain yield advantages under terminal drought in chickpea (*Cicer arietinum* L.). *Field. Crop. Res.* **201**, 146–161.

Rellan-Alvarez, R., Lobet, G., Lindner, H. *et al.* (2015) GLO-Roots: an imaging platform enabling multidimensional characterization of soil-grown root systems. *eLife*, **4**, 1–26. https://doi.org/10.7554/eLife.07597.002

Romero-Ramirez, F.J., Munoz-Salinas, R. and Medina-Carnicer, R. (2018) Speeded up detection of squared fiducial markers. *Image Vision Comput.* **76**, 38–47.

Sachs, J. (1865) *Handbuch der Experimental-Physiologie der Pflanzen*. Leipzig: Wilhelm Engelmann, pp. 1–536, vol 4. https://doi.org/10.5962/bhl.title.113036.

Sanders, J.L. and Brown, D.A. (1978) New fiber optic technique for measuring root-growth of soybeans under field conditions. *Agron. J.* **70**, 1073–1076.

Serraj, R., Krishnamurthy, L., Kashiwagi, J., Kumar, J., Chandra, S. and Crouch, J.H. (2004) Variation in root traits of chickpea (*Cicer arietinum* L.) grown under terminal drought. *Field. Crop. Res.* **88**, 115–127.

Shahzad, Z., Kellermeier, F., Armstrong, E.M., Rogers, S., Lobet, G., Amtmann, A. and Hills, A. (2018) EZ-Root-VIS: a software pipeline for the rapid analysis and visual reconstruction of root system architecture. *Plant Physiol.* **177**, 1368–1381.

Shrestha, R., Al-Shugeairy, Z., Al-Ogaidi, F., Munasinghe, M., Radermacher, M., Vandenhirtz, J. and Price, A.H. (2014) Comparing simple root phenotyping methods on a core set of rice genotypes. *Plant Biol.* **16**, 632–642.

Silva-Navas, J., Moreno-Risueno, M.A., Manzano, C., Pallero-Baena, M., Navarro-Neila, S., Tellez-Robledo, B., Garcia-Mina, J.M., Baigorri, R., Gallego, F.J. and del Pozo, J.C. (2015) D-Root: a system for cultivating plants with the roots in darkness or under different light conditions. *Plant J.* **84**, 244–255.

Slovak, R., Goschl, C., Su, X., Shimotani, K., Shiina, T. and Busch, W. (2014) A scalable open-source pipeline for large-scale root phenotyping of Arabidopsis. *Plant Cell*, **26**, 2390–2403.

Smith, S. and De Smet, I. (2012) Root system architecture: insights from Arabidopsis and cereal crops. *Philos. Trans. R Soc. Lond. B Biol. Sci.* **367**, 1441–1452.

Tian, X. and Doerner, P. (2013) Root resource foraging: does it matter? *Front Plant Sci.* **4**, 303.

Upadhyaya, H.D., Kashiwagi, J. *et al.* (2012) Phenotyping chickpeas and pigeonpeas for adaptation to drought. *Front. Physiol.* **3**, 179.

Vadez, V., Kholova, J., Medina, S., Kakkera, A. and Anderberg, H. (2014) Transpiration efficiency: new insights into an old story. *J. Exp. Bot.* **65**, 6141–6153.

Wang, Z.-G., Jin, X., Bao, X.-G., Li, X.-F., Zhao, J.-H., Sun, J.-H., Christie, P. and Li, L. (2014) Intercropping enhances productivity and maintains the most soil fertility properties relative to sole cropping. *PLoS One*, **9**, e113984.

Weiner, J., Du, Y.-L., Zhang, C., Qin, X.-L. and Li, F.-M. (2017) Evolutionary agroecology: individual fitness and population yield in wheat (*Triticum aestivum*). *Ecology*, **98**, 2261–2266.

Wu, J., Wu, Q., Pages, L., Yuan, Y., Zhang, X., Du, M., Tian, X. and Li, Z. (2018) RhizoChamber-Monitor: a robotic platform and software enabling characterization of root growth. *Plant Methods*, **14**, 44.

Yuan, P., Ding, G.D., Cai, H.M., Jin, K.M., Broadley, M.R., Xu, F.S. and Shi, L. (2016) A novel Brassica-rhizotron system to unravel the dynamic changes in root system architecture of oilseed rape under phosphorus deficiency. *Ann. Bot.* **118**, 173–184.

Zhang, Z.Y. (2000) A flexible new technique for camera calibration. *IEEE Trans. Pattern. Anal. Mac. Intell.* **22**, 1330–1334.